



Quantitative Image Analysis of HIV-1 Infection in Lymphoid Tissue

Ashley T. Haase; Keith Henry; Mary Zupancic; Gerald Sedgewick; Russell A. Faust; Holly Melroe; Winston Cavert; Kristin Gebhard; Katherine Staskus; Zhi-Qiang Zhang; Peter J. Dailey; Henry H. Balfour Jr.; Alejo Erice; Alan S. Perelson

Science, New Series, Vol. 274, No. 5289. (Nov. 8, 1996), pp. 985-989.

Stable URL:

<http://links.jstor.org/sici?sici=0036-8075%2819961108%293%3A274%3A5289%3C985%3AQIAOHI%3E2.0.CO%3B2-0>

Science is currently published by American Association for the Advancement of Science.

Your use of the JSTOR archive indicates your acceptance of JSTOR's Terms and Conditions of Use, available at <http://www.jstor.org/about/terms.html>. JSTOR's Terms and Conditions of Use provides, in part, that unless you have obtained prior permission, you may not download an entire issue of a journal or multiple copies of articles, and you may use content in the JSTOR archive only for your personal, non-commercial use.

Please contact the publisher regarding any further use of this work. Publisher contact information may be obtained at <http://www.jstor.org/journals/aaas.html>.

Each copy of any part of a JSTOR transmission must contain the same copyright notice that appears on the screen or printed page of such transmission.

The JSTOR Archive is a trusted digital repository providing for long-term preservation and access to leading academic journals and scholarly literature from around the world. The Archive is supported by libraries, scholarly societies, publishers, and foundations. It is an initiative of JSTOR, a not-for-profit organization with a mission to help the scholarly community take advantage of advances in technology. For more information regarding JSTOR, please contact support@jstor.org.

similar in structure, the putative input domains of CKI1 and ETR1 differ, suggesting separate functions. The simplest explanation of the *cki1* phenotype is that CKI1, acting as a cytokinin receptor, when overexpressed confers the ability on the expressing cells to sense low concentrations of endogenous cytokinin that is normally unable to trigger growth and shoot formation. Obviously, further work is required to define the function of CKI1, but it and ETR1 could represent members of a gene family that diverged to respond to different phytohormones.

REFERENCES AND NOTES

- R. Horgan, in *Advanced Plant Physiology*, M. B. Wilkins, Ed. (Pitman, London, 1984), pp. 53–75.
- F. Skoog and C. O. Miller, *Symp. Soc. Exp. Biol.* **11**, 118 (1957).
- A. N. Binns, *Annu. Rev. Plant Physiol. Plant Mol. Biol.* **45**, 173 (1994).
- H. Hayashi, I. Czaja, H. Lubenow, J. Schell, R. Walden, *Science* **258**, 1350 (1992).
- Arabidopsis* (ecotype Wassilewskija) was transformed by the procedure of K. Akama, H. Shiraishi, S. Ohta, K. Nakamura, and K. Okada [*Plant Cell Rep.* **12**, 7 (1992)], except that shoot-inducing medium was replaced by MS medium [T. Murashige and F. Skoog, *Physiol. Plant.* **15**, 473 (1962)] containing 1% sucrose, 1/100th volume of 5% 2-(*N*-morpholino)ethanesulfonic acid (adjusted to pH 5.7 with KOH), myo-inositol (100 mg/liter), thiamine-HCl (20 mg/liter), pyridoxine-HCl (1 mg/liter), and nicotinic acid (1 mg/liter), solidified with 0.3% Phytigel (Sigma) as the basal medium for regeneration of transgenic organs and for mutant screening. Antibiotics and plant hormones were added as described (6) (Fig. 3).
- The screenings for cytokinin-independent mutants were done as follows. Calli transformed with pPCVEn4HPT were cultured on basal medium (5) supplemented with hygromycin (40 mg/liter), cefotaxime (150 mg/liter), and vancomycin (100 mg/liter), at 23°C under continuous light (5000 lux) for 3 weeks. Calli that proliferated rapidly, turned green, and produced shoots were selected and subcultured on the same medium. These lines were maintained by subculturing on basal medium (5).
- T. Kakimoto, data not shown.
- DNA isolated from the *cki1-1* line was digested with Spe I, self-ligated, and used to transform *Escherichia coli* (DH10B) by electroporation, and the plasmid (pC1S1) was purified from the ampicillin-resistant *E. coli* cells as described elsewhere [C. Koncz *et al.*, in *Plant Molecular Biology Manual*, S. B. Gelvin and R. A. Schilperoort, Eds. (Kluwer Academic, Dordrecht, Netherlands, 1994), section B2].
- A Spe I digest of pC1S1 was ligated to the Xba I fragment of pPCVEn4HPT (4), which carries the T-DNA right border sequence, the vegetative (*oriV*), the conjugational (*oriT*) DNA replication origins of plasmid RK2, and the T-DNA left border sequence, to yield Ti plasmid pC1S1Ti.
- RNA from the *cki1-1* line was reverse-transcribed with the sequence-specific primer 5'-AGGCGTC-CATTCAGCTTGAATGG. The cDNA was amplified by polymerase chain reaction with a 5' primer (5'-AGATCGCACCATTGTTGTTTGTAGC) and a 3' primer (5'-CACACAAACCATACAGGCCAACCG), whose sequences were based on the genomic sequence. The amplified DNA was used to screen a cDNA library that had been constructed in Lambda ZAP II (Stratagene), in accordance with the manufacturer's instructions, with polyadenylated [poly(A)⁺] RNA from shoot tissue of the *cki1-1* line. Eighteen positive plaques were identified among 2 × 10⁵ plaques, and both ends of the five longest clones were sequenced. All of the sequences determined from the 5' ends were found in pC1S1. Of the five clones, cCKI1-16 was used for subsequent experiments. Both strands of cCKI1-16 were sequenced, and the complete sequence of cCKI1-16 was present in pC1S1 with the exception of the 3' noncoding region. cCKI1-16 contained 186 bp of 5' noncoding sequence, 3366 bp of coding sequence, and 143 bp of 3' noncoding sequence including poly(A). The DNA Data Bank of Japan accession number for the nucleotide sequence of the cDNA is D87545.
- For construction of the Ti plasmid carrying *CK11* cDNA linked to the CaMV 35S RNA promoter, 157 bp of the 5' noncoding sequence of cCKI1-16 was removed by treatment with exonuclease III, and all of the 3' noncoding sequence was removed by digestion with Spe I (the stop codon is at the Spe I site). The remaining sequence, together with the 34-bp vector sequences flanking the 5' end of the cDNA, was blunt-end cloned into the Sma I site of pMON530 [S. G. Rogers, H. J. Klee, R. B. Fraley, *Methods Enzymol.* **153**, 253 (1987)] next to the CaMV 35S RNA promoter, and the plasmid that contained the insert in the sense orientation was selected and designated p35ScCKI1.
- Five micrograms of poly(A)⁺ RNA was used for each lane.
- The DNA region from the 5' end of the Pst I site at nucleotide 2652 was used as a probe. Hybridization was done in 5 × SSPE (750 mM NaCl, 5 mM EDTA, 50 mM sodium phosphate, pH 7.4) that contained sheared salmon sperm DNA (200 µg/ml) and 0.2% SDS at 68°C; washing was done in 0.5 × SSPE containing 0.2% SDS at 65°C.
- E. M. Meyerowitz, in *Methods in Arabidopsis Research*, C. Koncz, N.-H. Chua, J. Schell, Eds. (World Scientific, Singapore, 1992), pp. 100–118.
- J. S. Perkinson and E. C. Kofoid, *Annu. Rev. Genet.* **26**, 71 (1992).
- J. B. Stock, A. J. Ninfa, A. M. Stock, *Microbiol. Rev.* **53**, 450 (1989).
- E. M. Hrabak and D. K. Willis, *J. Bacteriol.* **174**, 3011 (1992).
- S. Nagasawa, S. Tokishita, H. Aiba, T. Mizuno, *Mol. Microbiol.* **6**, 799 (1992).
- I. M. Ota and A. Varshavsky, *Science* **262**, 566 (1993).
- T. Maeda, S. M. Wurgler-Murphy, H. Saito, *Nature* **369**, 242 (1994).
- C. Chang, S. F. Kwok, A. B. Bleeker, E. M. Meyerowitz, *Science* **262**, 539 (1993).
- N. Wang, G. Shaulsky, R. Escalante, W. F. Loomis, *EMBO J.* **15**, 3890 (1996).
- J. Hua, C. Chang, Q. Sun, E. M. Meyerowitz, *Science* **269**, 1712 (1995).
- J. Q. Wilkinson, M. B. Lanahan, H.-C. Yen, J. J. Giovannoni, H. J. Klee, *ibid.* **270**, 1807 (1995).
- G. E. Schaller and A. B. Bleeker, *ibid.*, p. 1809.
- Single-letter abbreviations for the amino acid residues are as follows: A, Ala; C, Cys; D, Asp; E, Glu; F, Phe; G, Gly; H, His; I, Ile; K, Lys; L, Leu; M, Met; N, Asn; P, Pro; Q, Gln; R, Arg; S, Ser; T, Thr; V, Val; W, Trp; and Y, Tyr.
- I thank D. Collings for correcting the English and for commenting on the manuscript, H. Shibaoka for extensive support, H. Hayashi for advice, and Y. Shinzaki for critical reading of the manuscript. Special thanks are due to R. Walden for providing plasmid pPCVEn4HPT, for comments on the manuscript, and for continuous encouragement. pMON530 was supplied by Monsanto. Supported in part by Grants-in-Aid for Scientific Research on Priority Areas (The Molecular Basis of Flexible Organ Plans in Plants, number 06278103) and grants from the Nissan Foundation and the Sumitomo Foundation.

11 June 1996; accepted 5 September 1995

Quantitative Image Analysis of HIV-1 Infection in Lymphoid Tissue

Ashley T. Haase,* Keith Henry, Mary Zupancic, Gerald Sedgewick, Russell A. Faust, Holly Melroe, Winston Cavert, Kristin Gebhard, Katherine Staskus, Zhi-Qiang Zhang, Peter J. Dailey, Henry H. Balfour Jr., Alejo Erice, Alan S. Perelson

Tracking human immunodeficiency virus–type 1 (HIV-1) infection at the cellular level in tissue reservoirs provides opportunities to better understand the pathogenesis of infection and to rationally design and monitor therapy. A quantitative technique was developed to determine viral burden in two important cellular compartments in lymphoid tissues. Image analysis and *in situ* hybridization were combined to show that in the presymptomatic stages of infection there is a large, relatively stable pool of virions on the surfaces of follicular dendritic cells and a smaller pool of productively infected cells. Despite evidence of constraints on HIV-1 replication in the infected cell population in lymphoid tissues, estimates of the numbers of these cells and the virus they could produce are consistent with the quantities of virus that have been detected in the bloodstream. The cellular sources of virus production and storage in lymphoid tissues can now be studied with this approach over the course of infection and treatment.

Viral burden is a critical measure of the progress of HIV-1 infection (1), but there is as yet little information about the magnitude of infection in cellular compartments in lymphoid tissue (LT) where virus is produced and persists (2–4). A portion of the viral load in LT is associated with mononuclear cells (MNCs) such as CD4⁺ T lymphocytes,

monocytes, and macrophages in which viral RNA is readily detected. Virus production, and loss of CD4⁺ T cells from the cytopathic effects of viral replication or elimination by immune surveillance, can be directly attributed to this population, and it is this population that should diminish in response to current antiretroviral treatments that block

new infections. Another significant fraction of viral load in LT is associated with follicular dendritic cells (FDCs). These cells bind virions on their surfaces in immune complexes (5) and could slow systemic spread of HIV through this entrapment mechanism (6). Retention of infectivity of HIV-1 associated with FDCs suggests (7), however, that this compartment could be a continuing source of infection as well. To investigate the contributions and response of each cellular compartment to pathogenesis and treatment, we developed an approach to quantitating viral burden in the MNC and FDC compartments.

We used viral RNA as the measure of viral burden and quantitated and distinguished viral RNA in MNCs from viral RNA encapsidated in virions on the surfaces of FDCs by *in situ* hybridization (8). HIV RNA in viral particles distributed over the processes of FDCs generates a diffuse hybridization signal in germinal centers (GCs), whereas the intracellular signal for MNCs is discretely localized to individual cells (1, 5). To quantitate viral RNA in these cellular compartments, we used radioactively labeled RNA probes to generate hybridization signals in autoradiographs of silver grains overlying MNCs or associated with FDCs. We then calculated the number of copies of viral RNA from the number of silver grains, the specific activity of the probes, the length of autoradiographic exposure, and the efficiency of silver grain formation (9).

To count the silver grains overlying MNCs or FDCs, we used quantitative image analysis (10). The color video image of a field with an infected MNC is shown in Fig. 1A. The silver grains illuminated by trans- and epipolarized light are yellow-green in color and are scattered randomly or tightly clustered over infected cells such as the one indicated by the arrow. The image was simplified for counting grains by illuminating

the field with epipolarized light alone so that the silver grains and other highly reflective objects stand out, as is evident in the black-and-white video image in Fig. 1B. The red overlay in Fig. 1C highlights the silver grains in the field, and the white line traces the outline of the infected cell and the silver grains to be measured. Each silver grain occupies a specific number of picture elements, or pixels, and it is the area of the grains in pixels that is measured. To convert this area to grain counts, we previously determined the standard area (in pixels) of a silver grain at a particular magnification. We found, for example, by manually counting the grains over a MNC like the one shown in Fig. 1 that at a magnification of $\times 400$, a standard area parameter of 2.5 accurately converted areas in pixels to grain counts. This value was subsequently used to automatically score the number of silver grains over cells.

We validated this approach by applying it, under conditions comparable with those used in tissue sections, to cells in which the number of copies of HIV-1 full-length RNA had been previously determined. By com-

paring Northern blot analysis of extracted RNA with oligonucleotide probes specific for full-length, singly spliced, and multiply spliced viral RNAs, ACH-2 cells had been shown (11) to contain 300 to 400 copies of full-length viral RNA. We injected ACH-2 cells into a mouse spleen and fixed and processed paraffin-embedded tissues as described (8). We counted silver grains over 100 ACH-2 cells in images of tissue sections of the spleen and also determined a mean number of 350 copies of full-length viral RNA per cell.

To count silver grains overlying FDCs in GCs, we captured video images of entire GCs at a relatively low magnification (original magnification, $\times 160$) (Fig. 1D). To determine the standard area conversion factor at this magnification, we accurately determined the number of silver grains in segments of the GCs, indicated in Fig. 1D by the white lines, by manually counting the grains at high magnification ($\times 600$). From the number of silver grains in the entire GC, reconstructed from individual segments, we found that a standard area factor of 1.2 would convert the area of

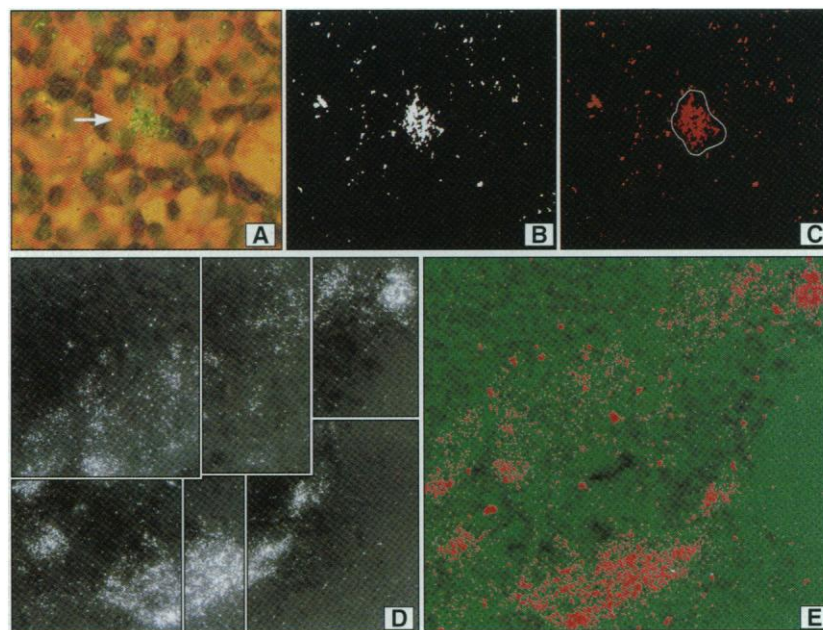


Fig. 1. Quantitative image analysis of HIV RNA in LT. **(A)** A MNC with HIV RNA (indicated by the arrow) in an autoradiograph of a section of tonsil (bright-field and epipolarized illumination, original magnification, $\times 400$). The specular reflectance from the silver grains imparts a yellow-green color to the grains. **(B)** High-contrast black and white image of the same field illuminated with epipolarized light. Only silver grains and other highly reflective objects in the section relevant to the analysis stand out. **(C)** For computer-assisted analysis, the image is digitized into 512 by 480 pixels. The area (in squared pixels) occupied by the silver grains in the image is measured after the grains are marked with the MetaMorph threshold tool, which overlays objects in red whose gray values are less than the threshold value set with the tool. The tracing tool is used to delineate the region of silver grains overlying the infected cell that will be measured (white trace). **(D)** Black and white video image of HIV RNA in virions associated with FDCs in a GC in a section of tonsil (epipolarized illumination). To include the entire GC, the image was captured at $\times 160$. Silver grains were counted at $\times 600$ in segments of the GC (delineated by the white lines) and summed to accurately determine the number in the entire GC. **(E)** Silver grains in the GC highlighted by a red overlay from the MetaMorph threshold tool.

A. T. Haase, M. Zupancic, W. Cavert, K. Gebhard, K. Staskus, Z.-Q. Zhang, Department of Microbiology, University of Minnesota Medical School, Minneapolis, MN 55455, USA.

K. Henry and H. Melroe, HIV Program, St. Paul-Ramsey Medical Center, St. Paul, MN 55101, USA, and Department of Medicine, University of Minnesota Medical School, Minneapolis, MN 55455, USA.

G. Sedgewick, Department of Cell Biology and Neuroanatomy, University of Minnesota Medical School, Minneapolis, MN 55455, USA.

R. A. Faust, Department of Otolaryngology, University of Minnesota Medical School, Minneapolis, MN 55455, USA.

P. J. Dailey, Chiron Corporation, Emeryville, CA 94608, USA.

H. H. Balfour Jr. and A. Erice, Department of Laboratory Medicine and Pathology, University of Minnesota Medical School, Minneapolis, MN 55455, USA.

A. S. Perelson, Theoretical Biology and Biophysics, Los Alamos National Laboratory, Los Alamos, NM 87545, USA.

*To whom correspondence should be addressed.

grains highlighted by a red overlay in Fig. 1E to grain counts. After this standard area parameter had been validated in this way in several GCs, we used it to score silver grains automatically in images with a magnification of $\times 160$ of positive GCs.

We assessed the sensitivity and specificity of the assay by comparing the signals generated through in situ hybridization with antisense and sense HIV-1 RNA probes. Because the tissue sections are not denatured before

hybridization, viral DNA sequences are not available for hybridization and the amount of nonspecific hybridization can be ascertained from the hybridization signal generated by the sense probe. For the autoradiographic exposure time of 24 hours that we used to maintain the clear discrimination between the signal from FDCs and MNCs, the background over MNCs and GCs detected with the sense probe was negligible; the limit of detection with the antisense probe was about 20 copies

of viral RNA per cell. The assay of viral RNA in the FDC or MNC pool was also reproducible, varying $\leq 15\%$ in independent measurements of individual MNCs or GCs (12).

To compare cellular pools of viral RNA in different LTs and to estimate total-body viral burden, we estimated the weight of the relevant LT in the tissue sections. More than 90% of the tonsillar biopsy tissue was composed of LT (Fig. 2A), whereas in tissue sections of spleen the white pulp with GCs

Table 1. In situ hybridization and quantitative image analysis of HIV-1 RNA levels in LT. LTs were obtained from HIV-1-infected individuals in the Centers for Disease Control and Prevention (CDC) clinical stage shown and with the CD4 counts indicated. Tissues were fixed immediately to eliminate autolysis as a variable by immersion for 4 to 5 hours in 4% paraformaldehyde, or for at least 24 hours in Streck's tissue fixative, followed by transfer to 70 to 80% ethanol and paraffin embedding. In preliminary experiments, these procedures for tissue processing were determined to be optimal and comparable for detection of HIV RNA and preservation of cellular morphology. The number of copies of HIV-1 RNA was determined by in situ hybridization and quantitative image analysis. HIV-1 RNA levels per milliliter of plasma were determined by branched DNA (bDNA) assay (22) in samples taken at the time of tonsil biopsy (patients 4 through 7 were biopsied several times as indicated). The viral clearance rate, cV , which under quasi-steady-state conditions should equal viral production, was calculated assuming $c = 3 \text{ day}^{-1}$ (19) and that V is the total viral load in extracellular fluid calculated by dividing the number of HIV RNA equivalents per milliliter of plasma by 2 and then multiplying by the $15 \times 10^3 \text{ ml}$ of extracellular fluid in a 70-kg individual. The rate of virus production in LT, $N\delta T^*$, was calculated assuming that N is about equal to the maximum of the range of the number of copies of HIV RNA per MNC divided by 2. T^* was taken to be the frequency of productively infected MNCs per gram of tissue multiplied by the assumed 700 g of LT per 70-kg individual, and $\delta = 0.5 \text{ day}^{-1}$ (19). N , T^* , and c will be underestimates because, respectively, only about 75% of a productively infected MNC will be analyzed in an 8- μm section, because T^* does not include infected cells with fewer than 20 copies of viral RNA, and because of the methods used to estimate c (19). 3TC, Lamivudine-Epivir; D4T, Stavudine-Zerit; DDC, Zalcitabine-HIVID; DLV, Delavirdine; ZDV, Zidovudine-Retrovir. Dashes indicate not applicable.

CDC class	Treatment	CD4 count/ mm ³ of blood	Sample	Number of HIV RNA equivalents/ml of plasma (bDNA assay)	Number of copies of HIV RNA/g of tissue		Average number (and range) of copies of HIV RNA per MNC	Frequency of productively infected MNCs/g of tissue	$cV/N\delta T^*$
					FDCs	MNCs			
<i>Patient number 1 (age 26 years)</i>									
B3	ZDV + 3TC	114	Tonsil, right	4×10^4	2.3×10^8	2.4×10^6	62 (20-188)	3.8×10^4	0.7
	ZDV + 3TC	-	Tonsil, left	-	4.9×10^8	3.9×10^6	86 (30-259)	4.5×10^4	-
<i>Patient number 2 (age 32 years)</i>									
A2	ZDV + DLV	375	Tonsil, right	$<5 \times 10^3$	1.6×10^8	2.9×10^6	73 (26-130)	4×10^4	-
	ZDV + DLV	-	Tonsil, left	-	9.2×10^7	1.9×10^6	58 (36-118)	3.3×10^4	-
<i>Patient number 3 (age 31 years)</i>									
A1	ZDV	638	Tonsil	$<5 \times 10^3$	3.2×10^8	8.6×10^5	62 (23-140)	1.4×10^4	-
<i>Patient number 4 (age 45 years)</i>									
A1	None	551	Tonsil, baseline	10^4	1.9×10^8	1.6×10^6	76 (28-214)	2×10^4	0.3
	None	-	Tonsil, +1 month	-	1.6×10^8	1.3×10^5	79 (24-234)	1.6×10^3	-
	None	763	Tonsil, +6 months	$<5 \times 10^3$	5.4×10^8	4.6×10^5	150 (20-287)	3×10^3	-
	None	-	Tonsil, +12 months	-	4.3×10^8	1.4×10^7	79 (21-188)	1.8×10^5	-
	None	437	Tonsil, +14 months	1.4×10^4	3.4×10^8	4×10^6	94 (20-180)	4.2×10^4	0.2
<i>Patient number 5 (age 32 years)</i>									
A2	ZDV	294	Tonsil, baseline	$<5 \times 10^3$	10^8	8×10^4	80 (20-97)	10^3	-
	ZDV	-	Tonsil, +1 month	-	6.2×10^7	8×10^4	80 (20-108)	10^3	-
	ZDV + DLV	215	Tonsil, +6 months	$<5 \times 10^3$	6.3×10^7	7.5×10^4	75 (49-91)	10^3	-
	None	202	Tonsil, +12 months	$<5 \times 10^3$	7×10^7	3×10^6	58 (20-151)	5.1×10^4	-
	None	197	Tonsil, +14 months	$<5 \times 10^3$	5×10^7	3.4×10^6	57 (20-106)	6×10^4	-
<i>Patient number 6 (age 32 years)</i>									
A1	None	633	Tonsil, baseline	7.6×10^4	2.3×10^7	3.9×10^6	38 (20-141)	10^5	0.7
	None	-	Tonsil, +1 month	-	1.3×10^7	2.2×10^6	72 (20-177)	3×10^4	-
	ZDV + DDC	389	Tonsil, +12 months	$<5 \times 10^3$	5.8×10^7	1.7×10^6	41 (20-115)	4×10^4	-
<i>Patient number 7 (age 48 years)</i>									
A1	ZDV	782	Tonsil, baseline	2.6×10^4	4.2×10^6	1.8×10^6	124 (48-222)	1.5×10^4	1
	ZDV	-	Tonsil, +1 month	-	7.6×10^7	1.9×10^7	74 (20-183)	2.6×10^5	-
	ZDV	778	Tonsil, +6 months	2.9×10^4	1.8×10^8	6×10^5	85 (50-188)	7.1×10^3	2.8
	ZDV	615	Tonsil, +14 months	7.6×10^4	3.2×10^7	10^7	44 (20-136)	2.3×10^5	0.3
<i>Patient number 8 (age 37 years)</i>									
A3	D4T	140	Spleen	$<5 \times 10^3$	7.9×10^6	1.8×10^5	58 (45-77)	3.1×10^3	-
<i>Patient number 9 (age 39 years)</i>									
A2	DDC	245	Lymph node	$<5 \times 10^3$	3.8×10^7	1.1×10^6	63 (28-124)	1.7×10^4	-
	None	106	Spleen	2×10^5	7×10^7	5.7×10^6	63 (20-128)	9×10^4	2.2
Mean		402			1.5×10^8	3.4×10^6	74	5.3×10^4	1.0

made up only 10 to 20% of the sample (Fig. 2B). We converted the data from image analysis to copies of viral RNA per gram of LT from the determined areas, nominal thickness (8 μm), and our determination of the density of fixed LT specimens ($\sim 1 \text{ g/cm}^3$).

We used quantitative image analysis and in situ hybridization to assess HIV burden in cellular compartments in LT in blinded cross-sectional and longitudinal studies of nine HIV-1-infected individuals (Table 1). These individuals were largely asymptomatic and, with one exception, were receiving antiretroviral treatment (Table 1). We focused in seven of the nine cases on LT obtained by biopsy of tonsillar tissue because tonsil is an

accessible source of LT that can be biopsied frequently and repeatedly in an outpatient clinic setting (13). We also analyzed spleen and lymph node tissues from one individual, and spleen from another.

In the presymptomatic stage of infection, we found that the amount of HIV-1 RNA associated with FDCs exceeded the amount of viral RNA in the infected MNC population by 10- to 40-fold. Because most of the HIV-1 RNA is in the FDC compartment, the number of copies of viral RNA in the FDC pool determined by image analysis of sections and by measuring viral RNA in tissue extracts should be in reasonable agreement. In two individuals from whom we obtained simultaneous samples of right and left tonsil, the

concentration of viral RNA in the samples determined by branched DNA assay and by image analysis agreed within the approximate two- to threefold variation between samples (Table 2).

The size of the FDC pool was not related to clinical stage, CD4 count, or treatment. The relative magnitude of the FDC pool can be appreciated by comparisons of the concentration of viral RNA in LT and in blood. The concentration of viral RNA in the FDC pool exceeded concentrations of viral RNA in plasma by factors of 10^2 to $>10^4$ and, at times when the concentration of viral RNA in plasma was below the detection level of the assay (5×10^3 copies per milliliter), there were $>10^6$ copies of viral RNA per gram of LT in the FDC pool (Table 1).

In four individuals from whom sequential tonsillar biopsies were obtained over the course of more than 1 year (patients 4 to 7 in Table 1), the concentration of HIV RNA associated with FDCs ranged from $\sim 10^7$ to $>10^8$ copies per gram and rarely exceeded 5×10^8 copies per gram. Although considerable variation at different times and at different sites might have been expected, the FDC pool was relatively stable and was comparable in tonsil, lymph node, and spleen samples from the same or different individuals. We based estimates of total-body burden of $\sim 10^{11}$ copies of HIV RNA associated with FDCs on a 70-kg individual in which LT is 1% of the total body weight (14) and justified the extrapolation by the relative homogeneity of the pool. Our estimates are consistent with a large but saturable pool of virus with the potential to perpetuate infection, but also with virus with restricted access to the whole population of susceptible host cells (6, 7).

There was also no relation between the size of the MNC pool or the number of infected cells and clinical status, CD4 count, or treatment (Table 1). The mean (74) and maximum numbers of copies per infected cell in LT ($\sim \leq 250$ copies per cell) were considerably less than in ACH-2 cells (11) or peripheral blood mononuclear cells (PBMCs) infected in culture: the mean in the PBMC culture was 1100 copies per cell and the maximum was 3800 copies per cell (15). The reduced amounts of viral RNA in vivo in most MNCs and the low frequency of cells with >250 copies of viral RNA in LT are consistent with the hypothesis that infected cells are eliminated by immune defenses with increasing probability at later stages of the viral life cycle, where the infected cells have higher concentrations of viral RNA, proteins, and particles. Alternatively, HIV gene expression in vivo might be suppressed by cytokines or factors elaborated by CD8^+ T cells (16), or might be restricted because the amounts of host cell viral gene products such as Tat or Rev in

Fig. 2. Determination of relevant LT areas by image analysis. (A) The MetaMorph tracing tool was used to trace (in red) a submucosal region of LT in a section of a tonsillar biopsy (original magnification, $\times 20$). The area in pixels was converted to area in millimeters by applying a calibration relating pixel area to square millimeters from a $\times 20$ image of a 2-mm scale with 0.1-mm divisions. (B) An area of white pulp in a section of spleen. The more darkly stained white pulp was identified and traced in color with the MetaMorph autotrace tool. The individual areas were summed to determine total area.

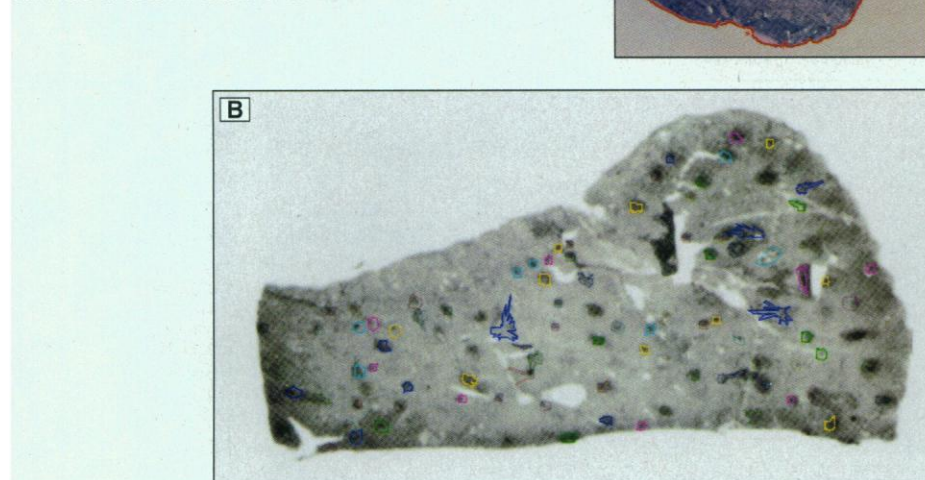


Table 2. Comparison of single-cell and population estimates of HIV-1 RNA. Simultaneous biopsies of right and left palatine tonsil were obtained and divided into two weighed fragments. One portion was snap frozen, and at a later time RNA was extracted and the number of HIV RNA equivalents determined by bDNA assay (22). The other portion was fixed and sectioned at a later time, and viral RNA associated with FDCs was quantitated as described in this report.

CDC class	Treatment	CD4 count/ mm^3 of blood	Sample	Number of copies of HIV RNA associated with FDCs/g of tonsillar tissue	
				In situ hybridization	bDNA assay
<i>Patient number 1 (age 26 years)</i>					
B3	ZDV + 3TC	110	Right tonsil	2.3×10^8	3.9×10^8
	ZDV + 3TC	110	Left tonsil	4.9×10^8	5.2×10^8
<i>Patient number 2 (age 32 years)</i>					
A2	ZDV + DLV	375	Right tonsil	1.6×10^8	8.1×10^7
	ZDV + DLV	375	Left tonsil	9.2×10^7	8.5×10^7

vivo are insufficient to support permissive replication (17).

We derived some preliminary estimates of the potential contribution of infected MNCs to the loss of CD4⁺ T lymphocytes and the production of virus in LT by combining the in situ "snapshots" of infection with turnover rates determined from studies of viral dynamics in the bloodstream (18, 19). The turnover of productively infected cells has been modeled by δT^* , in which $\delta \sim 0.5 \text{ day}^{-1}$ is the death rate of productively infected cells, and T^* is the number of productively infected cells (19). T^* can be estimated from the in situ snapshots to be about 5×10^4 cells per gram or about 4×10^7 cells in a 70-kg individual. This is an underestimate because there are 5 (2) to 10 (20) times as many CD4⁺ T lymphocytes with fewer than the limit of 20 copies of viral RNA per cell detected in these studies that might nevertheless be recognized and eliminated by immune surveillance mechanisms. Even if this were true, however, and we ignore the inclusion of monocytes and macrophages in the estimates of T^* , 2×10^8 CD4⁺ T lymphocytes at most would be lost per day in LT as a direct consequence of infection. This is lower than CD4⁺ T lymphocyte turnover calculated from dynamic studies (18, 19) and is consistent with CD4⁺ T cell depletion by mechanisms in addition to elimination of infected cells.

We also compared estimates of viral production inferred from measurements of plasma HIV-1 RNA over time with estimates from the putative site of production in LT. Perelson *et al.* (19) compute the steady-state rate of virus production from the rate of viral clearance from plasma (cV in Table 1) and model the rate of production by $N\delta T^*$, where N is the total number of virions produced by a productively infected cell during its lifetime. The relation of N to the intracellular RNA concentration is unknown, but in a typical lentivirus life cycle, most of the viral RNA is produced and the greatest fraction will be destined to be encapsidated in virions late in the cycle (21). We therefore approximated N as one-half of the maximum of the number of copies of HIV RNA per MNC (Table 1). With these assumptions, we find that cV is on average equal to $N\delta T^*$ (Table 1). Given the current uncertainties in estimating c , N , and T^* , this agreement is remarkable and suggests that when HIV is detectable in plasma, the concentrations accurately mirror production of virus at its site of generation in LT.

Image analysis of the presymptomatic stage of HIV-1 infection in LT revealed a relatively spatially homogeneous and temporally stable pool of virions associated with FDCs that exceeds the viral load in plasma by orders of magnitude. There was no evidence in this study of a response to treatment with inhibitors of reverse transcrip-

tion in either the FDC pool or the pool of productively infected cells. In future studies, it will be important to determine the magnitude and dynamics of infection in these cellular compartments throughout the course of infection and during treatment with more potent combinations of antiretroviral drugs. These studies should yield additional insights into pathogenesis and provide a rational basis for optimizing the timing and mix of antiviral treatments that will have the greatest effect on virus production and load in the principal tissue reservoirs.

REFERENCES AND NOTES

- J. W. Mellors *et al.*, *Science* **272**, 1167 (1996).
- J. Embretson *et al.*, *Nature* **362**, 359 (1993).
- G. Pantaleo *et al.*, *ibid.*, p. 355.
- G. Pantaleo *et al.*, *Proc. Natl. Acad. Sci. U.S.A.* **88**, 9838 (1991).
- C. H. Fox *et al.*, *J. Infect. Dis.* **164**, 1051 (1991); K. Tenner-Rácz *et al.*, *AIDS* **2**, 299 (1988); H. Spiegel, H. Herbst, G. Niedobitek, H.-D. Foss, H. Stein, *Am. J. Pathol.* **140**, 15 (1992); J. Schmitz *et al.*, *J. Immunol.* **153**, 1352 (1994).
- G. Pantaleo and A. S. Fauci, *Annu. Rev. Immunol.* **13**, 487 (1995); B. F. Haynes, G. Pantaleo, A. S. Fauci, *Science* **271**, 324 (1996).
- S. L. Heath, J. G. Tew, A. K. Szakal, G. F. Burton, *Nature* **377**, 740 (1995).
- For in situ hybridization, sections of 8 μm were cut, adhered to silanized glass slides, and deparaffinized through xylene and graded alcohols. Before hybridization, the sections were treated as described previously [A. T. Haase, in *In Situ Hybridization. Applications in Neurobiology*, K. L. Valentino, J. H. Eberwine, J. D. Barchas, Eds. (Oxford Univ. Press, New York, 1987), pp. 197–219]. In brief, slides were immersed in 0.2 N HCl for 30 min, 0.15 M triethanolamine (pH 7.4) for 15 min, and 0.005% digitonin for 5 min, all at room temperature. The slides were then incubated for 15 min at 37°C in a buffered solution containing 2 mM CaCl₂ and proteinase K (5 $\mu\text{g}/\text{ml}$). We found that these pretreatments resulted in equivalent or higher signal over GCs than did higher concentrations of proteinase K, as had been described (5). After the slides were removed and washed, they were acetylated (0.25% acetic anhydride) for 10 min and then dehydrated through graded solutions of ethanol. The sections were then covered with hybridization solution [50% deionized formamide, 10% dextran SO₄, 0.6 M NaCl, yeast tRNA (0.4 mg/ml), and 1 \times Denhardt's medium in 20 mM Hepes buffer (pH 7.2) with 1 mM EDTA and 40 mM dithiothreitol (DTT)] containing 10⁵ cpm of ³⁵S-labeled riboprobe per microliter. The riboprobes (purchased from Lofstrand Labs Limited, Gaithersburg, MD, as sense or antisense transcripts of the cloned restriction fragments) were complementary to about 90% of the sequences in full-length HIV genomic RNA and were labeled to specific activities of 6 $\times 10^8$ to 8 $\times 10^8$ dpm/ μg by incorporation of ³⁵S-cytidine 5'-triphosphate (CTP). The hybridization solution with probe was sealed under a cover slip with rubber cement and the slides were incubated for 24 hours at 45°C. After the cover slips were removed, the slides were immersed in 5 \times standard saline citrate (SSC) and washed as follows: 5 \times SSC, 10 mM DTT, 42°C, 30 min; 2 \times SSC, 50% formamide, 10 mM DTT, 60°C, 20 min; 2 \times RWS (0.1 M tris-HCl, pH 7.5, 0.4 M NaCl, 50 mM EDTA), 10 min. The sections were then digested at 37°C with ribonucleases A (25 $\mu\text{g}/\text{ml}$) and T1 (25 $\mu\text{g}/\text{ml}$) in RWS for 30 min, washed at 37°C in RWS for 15 min, washed in 2 \times SSC at 37°C for 15 min, washed in 0.1 \times SSC at 37°C for 15 min, dehydrated through graded alcohols containing 0.3 M ammonium acetate, dried, and coated with Kodak NTB-2 emulsion. After autoradiographic exposures of 24 hours at 4°C, the slides were developed and
- stained for 1 min in Wright's stain.
- Assuming that the collection of antisense riboprobes used hybridizes with 100% efficiency and 1:1 stoichiometry, taking the efficiency of silver grain formation in tissue sections to be 0.5 g/dpm for ³⁵S [A. W. Rogers, *Techniques of Autoradiography* (Elsevier North-Holland, Amsterdam, ed. 3, 1979), pp. 102–103], it can be estimated that one full-length copy of HIV-1 virion RNA would generate a signal of 2.4 silver grains per 24-hour autoradiographic exposure.
- For image analysis, autoradiographs were illuminated with epipolarized light through use of a mercury light source and the differential interference cube of the Olympus B-max microscope. Video images were captured with a low-light cooled charge-coupled device (CCD) camera (Optronics TEC-470) and Image 1/MetaMorph version 2 software (Universal Imaging, Westchester, PA). Silver grains were differentiated and measured with the "threshold" and "measure object" tools of the MetaMorph software. The relevant GCs and MNCs in the image were delineated with the tracing tool. On the basis of analyses illustrated in Fig. 1, measurement parameters for standard areas in pixels were set at each magnification to obtain grain counts. Data were recorded on a Microsoft Excel spreadsheet.
- H. Peng *et al.*, *Virology* **206**, 16 (1995).
- Images of MNCs and GCs illustrated in Fig. 1 determined at high magnification were repeatedly analyzed independently by A. T. Haase, M. Zupancic, and K. Gebhard to determine the reproducibility of 10 to 15%.
- R. A. Faust *et al.*, *Otolaryngol. Head Neck Surg.* **114**, 593 (1996).
- P. Lydyard and C. Grossi, in *Immunology*, I. Roitt, J. Brostoff, D. Male, Eds. (Lippincott, Philadelphia, PA, 1989), pp. 2.1–2.18.
- Cultures of PBMCs from a seronegative individual were stimulated with phytohemagglutinin and infected with 0.1 median tissue culture infectious dose (TCID₅₀) of HIV-1. The number of copies of HIV-1 RNA per cell was determined 5 days later by quantitative image analysis and in situ hybridization.
- C. M. Walker, D. J. Moody, D. P. Stites, J. A. Levy, *Science* **234**, 1563 (1986); J. E. Brinckmann, G. Gaudernack, F. Vartdal, *J. Immunol.* **144**, 2961 (1990); C. M. Walker, A. L. Erickson, F. C. Hsueh, J. A. Levy, *J. Virol.* **65**, 5921 (1991); M. Baier, A. Werner, N. Bannert, K. Metzner, R. Kurth, *Nature* **378**, 563 (1995); F. Cocchi *et al.*, *Science* **270**, 1811 (1995); S. M. Wolinsky *et al.*, *ibid.* **272**, 537 (1996).
- T. M. Folks, J. Justement, A. Kinter, C. A. Dinarello, A. S. Fauci, *Science* **238**, 800 (1987); R. J. Pomerantz, D. Trono, M. B. Feinberg, D. Baltimore, *Cell* **61**, 1271 (1990); M. A. Garcia-Blanco and B. R. Cullen, *Science* **254**, 815 (1991); T. Seshamma, O. Bagasra, D. Trono, D. Baltimore, R. J. Pomerantz, *Proc. Natl. Acad. Sci. U.S.A.* **89**, 10663 (1992); L. Duan, J. W. Oakes, A. Ferraro, O. Bagasra, R. J. Pomerantz, *Virology* **199**, 474 (1994); M. Adams *et al.*, *Proc. Natl. Acad. Sci. U.S.A.* **91**, 3862 (1994); J. A. Zack *et al.*, *Cell* **61**, 213 (1990).
- X. Wei *et al.*, *Nature* **373**, 117 (1995); D. Ho *et al.*, *ibid.*, p. 123.
- A. S. Perelson, A. U. Neumann, M. Markowitz, J. M. Leonard, D. D. Ho, *Science* **271**, 1582 (1996).
- B. K. Patterson *et al.*, *ibid.* **260**, 976 (1993); G. J. Nuovo, F. Gallery, P. MacConnell, A. Braun, *Am. J. Pathol.* **144**, 659 (1994); G. J. Nuovo, A. Forde, P. MacConnell, R. Fahrwald, *ibid.*, p. 40.
- A. T. Haase *et al.*, *Virology* **119**, 399 (1982).
- C. Pachi *et al.*, *J. Acquired Immune Defic. Syndr.* **8**, 446 (1995); R. L. Dewar *et al.*, *J. Infect. Dis.* **170**, 1172 (1994); Y. Cao *et al.*, *AIDS Res. Hum. Retroviruses* **11**, 353 (1995).
- We thank S. Wietgreffe and the reviewers for helpful comments; C. O'Neill and T. Leonard for preparation of the manuscript and figures; and the Ramsey Foundation, the Santa Fe Institute, the Joseph P. and Jeanne M. Sullivan Foundation, and NIH (grants AI 28246, AI 27661 and RR 06555) for support. Portions of this work were done under the auspices of the U.S. Department of Energy.

11 April 1996; accepted 29 July 1996

LINKED CITATIONS

- Page 1 of 3 -



You have printed the following article:

Quantitative Image Analysis of HIV-1 Infection in Lymphoid Tissue

Ashley T. Haase; Keith Henry; Mary Zupancic; Gerald Sedgewick; Russell A. Faust; Holly Melroe; Winston Cavert; Kristin Gebhard; Katherine Staskus; Zhi-Qiang Zhang; Peter J. Dailey; Henry H. Balfour Jr.; Alejo Erice; Alan S. Perelson

Science, New Series, Vol. 274, No. 5289. (Nov. 8, 1996), pp. 985-989.

Stable URL:

<http://links.jstor.org/sici?sici=0036-8075%2819961108%293%3A274%3A5289%3C985%3AQIAOHI%3E2.0.CO%3B2-0>

This article references the following linked citations. If you are trying to access articles from an off-campus location, you may be required to first logon via your library web site to access JSTOR. Please visit your library's website or contact a librarian to learn about options for remote access to JSTOR.

References and Notes

¹ **Prognosis in HIV-1 Infection Predicted by the Quantity of Virus in Plasma**

John W. Mellors; Charles R. Rinaldo Jr.; Phalguni Gupta; Roseanne M. White; John A. Todd; Lawrence A. Kingsley

Science, New Series, Vol. 272, No. 5265. (May 24, 1996), pp. 1167-1170.

Stable URL:

<http://links.jstor.org/sici?sici=0036-8075%2819960524%293%3A272%3A5265%3C1167%3APIHIPB%3E2.0.CO%3B2-0>

⁴ **Lymphoid Organs Function as Major Reservoirs for Human Immunodeficiency Virus**

Giuseppe Pantaleo; Cecilia Graziosi; Luca Butini; Philip A. Pizzo; Steven M. Schnittman; Donald P. Kotler; Anthony S. Fauci

Proceedings of the National Academy of Sciences of the United States of America, Vol. 88, No. 21. (Nov. 1, 1991), pp. 9838-9842.

Stable URL:

<http://links.jstor.org/sici?sici=0027-8424%2819911101%2988%3A21%3C9838%3ALOFAMR%3E2.0.CO%3B2-X>

⁶ **Toward an Understanding of the Correlates of Protective Immunity to HIV Infection**

Barton F. Haynes; Giuseppe Pantaleo; Anthony S. Fauci

Science, New Series, Vol. 271, No. 5247. (Jan. 19, 1996), pp. 324-328.

Stable URL:

<http://links.jstor.org/sici?sici=0036-8075%2819960119%293%3A271%3A5247%3C324%3ATAUOTC%3E2.0.CO%3B2-F>

NOTE: *The reference numbering from the original has been maintained in this citation list.*

LINKED CITATIONS

- Page 2 of 3 -



¹⁶ **CD8 + Lymphocytes Can Control HIV Infection in vitro by Suppressing Virus Replication**

Christopher M. Walker; Dewey J. Moody; Daniel P. Stites; Jay A. Levy
Science, New Series, Vol. 234, No. 4783. (Dec. 19, 1986), pp. 1563-1566.

Stable URL:

<http://links.jstor.org/sici?sici=0036-8075%2819861219%293%3A234%3A4783%3C1563%3ACLCHI%3E2.0.CO%3B2-F>

¹⁶ **Identification of RANTES, MIP-1a, and MIP-1b as the Major HIV-Suppressive Factors Produced by CD8+ T Cells**

Fiorenza Cocchi; Anthony L. DeVico; Alfredo Garzino-Demo; Suresh K. Arya; Robert C. Gallo; Paolo Lusso

Science, New Series, Vol. 270, No. 5243. (Dec. 15, 1995), pp. 1811-1815.

Stable URL:

<http://links.jstor.org/sici?sici=0036-8075%2819951215%293%3A270%3A5243%3C1811%3AIORMAM%3E2.0.CO%3B2-D>

¹⁶ **Adaptive Evolution of Human Immunodeficiency Virus-Type 1 During the Natural Course of Infection**

Steven M. Wolinsky; Bette T. M. Korber; Avidan U. Neumann; Michael Daniels; Kevin J. Kunstman; Amy J. Whetsell; Manohar R. Furtado; Yunzhen Cao; David D. Ho; Jeffrey T. Safrit; Richard A. Koup

Science, New Series, Vol. 272, No. 5261. (Apr. 26, 1996), pp. 537-542.

Stable URL:

<http://links.jstor.org/sici?sici=0036-8075%2819960426%293%3A272%3A5261%3C537%3AAEOHIV%3E2.0.CO%3B2-S>

¹⁷ **Cytokine-Induced Expression of HIV-1 in a Chronically Infected Promonocyte Cell Line**

Thomas M. Folks; Jesse Justement; Audrey Kinter; Charles A. Dinarello; Anthony S. Fauci
Science, New Series, Vol. 238, No. 4828. (Nov. 6, 1987), pp. 800-802.

Stable URL:

<http://links.jstor.org/sici?sici=0036-8075%2819871106%293%3A238%3A4828%3C800%3ACEOHIA%3E2.0.CO%3B2-O>

¹⁷ **Molecular Basis of Latency in Pathogenic Human Viruses**

Mariano A. Garcia-Blanco; Bryan R. Cullen

Science, New Series, Vol. 254, No. 5033. (Nov. 8, 1991), pp. 815-820.

Stable URL:

<http://links.jstor.org/sici?sici=0036-8075%2819911108%293%3A254%3A5033%3C815%3AMBOLIP%3E2.0.CO%3B2-N>

LINKED CITATIONS

- Page 3 of 3 -



¹⁷ Blocked Early-Stage Latency in the Peripheral Blood Cells of Certain Individuals Infected with Human Immunodeficiency Virus Type 1

Thikkavarapu Seshamma; Omar Bagasra; Didier Trono; David Baltimore; Roger J. Pomerantz
Proceedings of the National Academy of Sciences of the United States of America, Vol. 89, No. 22.
(Nov. 15, 1992), pp. 10663-10667.

Stable URL:

<http://links.jstor.org/sici?sici=0027-8424%2819921115%2989%3A22%3C10663%3ABELITP%3E2.0.CO%3B2-X>

¹⁷ Cellular Latency in Human Immunodeficiency Virus-Infected Individuals with High CD4 Levels can be Detected by the Presence of Promoter-Proximal Transcripts

Melanie Adams; Lamia Sharmeen; Jaculyn Kimpton; Joseph M. Romeo; J. Victor Garcia; B. Matija Peterlin; Mark Groudine; Michael Emerman
Proceedings of the National Academy of Sciences of the United States of America, Vol. 91, No. 9.
(Apr. 26, 1994), pp. 3862-3866.

Stable URL:

<http://links.jstor.org/sici?sici=0027-8424%2819940426%2991%3A9%3C3862%3ACLIHIV%3E2.0.CO%3B2-Y>

¹⁹ HIV-1 Dynamics in Vivo: Virion Clearance Rate, Infected Cell Life-Span, and Viral Generation Time

Alan S. Perelson; Avidan U. Neumann; Martin Markowitz; John M. Leonard; David D. Ho
Science, New Series, Vol. 271, No. 5255. (Mar. 15, 1996), pp. 1582-1586.

Stable URL:

<http://links.jstor.org/sici?sici=0036-8075%2819960315%293%3A271%3A5255%3C1582%3AHDIVVC%3E2.0.CO%3B2-C>

²⁰ Detection of HIV-1 DNA and Messenger RNA in Individual Cells by PCR-Driven in Situ Hybridization and Flow Cytometry

Bruce K. Patterson; Michele Till; Patricia Otto; Charles Goolsby; Manohar R. Furtado; Lincoln J. McBride; Steven M. Wolinsky
Science, New Series, Vol. 260, No. 5110. (May 14, 1993), pp. 976-979.

Stable URL:

<http://links.jstor.org/sici?sici=0036-8075%2819930514%293%3A260%3A5110%3C976%3ADOHDAM%3E2.0.CO%3B2-Y>